



# A transient analysis of incompressible fluid flow in vessels with moving boundaries

Analysis of incompressible fluid flow

833

Tony W.H. Sheu and Harry Y.H. Chen  
*Department of Naval Architecture and Ocean Engineering, National Taiwan University, Taipei, Taiwan, Republic of China*

Received November 1998

Revised June 1999

Accepted July 1999

**Keywords** *Finite element analysis, Transformation, Boundary conditions, Grids*

**Abstract** *We present in this paper a finite element analysis of Navier-Stokes equations in a time-varying domain. The method of weighted residuals is used together with the semi-discretization approach to obtain the discrete equations. In this approach, where the physical domain is allowed to vary, care is taken to retain the space conservation law property. We describe in detail the transformation of equations between fixed and moving grids. The validity of this method has been tested against two problems which are amenable to analytic solutions. Time accurate results show favorable agreement with analytic solutions. Having verified the applicability of the Galerkin finite element code to problems involving moving grids, we consider the fluid flow in a vessel, where a portion of its boundary moves in time. Results are presented with emphasis on the depiction of vortical flow details.*

## Introduction

Flow with moving boundaries can be encountered in many practical cases. Among the representative examples that have been studied in detail is the flow in internal combustion engines. Ship flow subject to changes in free surface elevation is another type of problem worthy of study and has attracted a great deal of research interest in recent years. The common feature of these flows is that the physical boundary is a part of the solution procedures. This adds additional complexity to the modeling of flow physics from the working equations. With the advent of faster computers and ever-improving numerical methods, it is now possible to tackle transient flow in a domain delineated by time-varying boundaries. The goal for the present investigation was to understand incompressible fluid flow in a flexible vessel. This problem is haemodynamically important in that shear stress exerted by flowing blood on the arterial wall has an essential effect on the early stage of atherosclerosis formation (Ku *et al.*, 1985). Detailed knowledge about the unsteady flow separation in a time-varying blood vessel is, thus, needed. As a necessary step towards extending the scope of blood flow simulation (Sheu *et al.*, 1999), we are prompted to conduct analysis on moving grids in the hope of simulating complex haemodynamics such as that considered in Taylor *et al.* (1998).

While many numerical solution algorithms have been developed for simulating unsteady flows in the literature, problems involving moving boundaries have been considered by relatively few authors. Early works

devoted to tackling problems with moving boundaries are detailed in Demirdizic and Peric (1990). The solution for this class of problems is best analyzed in non-Eulerian (moving) coordinates. To this end, one can derive the corresponding conservation equations in moving coordinates through transformation of variables. These field equations can be derived more straightforwardly in general moving coordinates under the concept of the Lie derivative (Satoru and Tomiko, 1987; Schouten, 1954). The grid fitted to the body moves in time and is not fixed in space. For analyses conducted in moving grids, it is important to incorporate the space conservation law (SCL) into the formulation (Trulio and Trigger, 1961). As the name indicates, the SCL relates the change of an elementary computational cell to the coordinate frame velocity. Failure to satisfy the space conservation law will cause the artificial mass to accumulate or diminish. Thomas and Lombard (1979) were among the first to recognize the need for solving this equation simultaneously with other conservation equations. Demirdizic and Peric (1983) later provided computational evidence to justify the rational use of the SCL equation as a constraint to simulate problems on non-stationary grids. In the present study, we adopted the concept of a moving grid in the finite element analysis.

The remainder of this paper is organized as follows. The next section is intended to derive working equations on moving grids. The finite element discretization method is briefly outlined. We then provide an analytic verification of the applicability of the code implemented on moving grids. For the sake of description, we use the convection-diffusion equation to benchmark our proposed scheme. This is followed by consideration of an analytic test problem for the solution of Navier-Stokes equations. In the result section, we present the numerical simulation of incompressible fluid flow in a vessel which partly undergoes a large-amplitude oscillation. Finally, we conclude with some remarks.

### Mathematical model

Most of the flow problems of engineering interest fall into the incompressible flow category. The governing equations for an unsteady, incompressible viscous flow in grids fixed in space are as follows:

$$u_x + v_y = 0 , \tag{1}$$

$$u_t + u u_x + v u_y = -p_x + \mu ( u_{xx} + u_{yy} ) , \tag{2}$$

$$v_t + u v_x + v v_y = -p_y + \mu ( v_{xx} + v_{yy} ) . \tag{3}$$

The above primitive-variable formulation involves use of a velocity vector and pressure as working variables for a fluid with kinematic viscosity  $\mu$ . The main reason for adopting equations (1-3) is that this primitive variable formulation accommodates closure initial and boundary conditions (Ladyzhenskaya, 1969). For accuracy reasons, adaptation of grid lines to the flow direction is desirable when simulating a flow which is unsteady in nature. Under these circumstances, movement of grid lines warrants careful consideration in flux

discretization conducted in between two consecutive time steps. To describe the method, we will consider the prototype equation of (2)-(3), namely, the scalar transport equation:

$$\phi_t + u \phi_x + v \phi_y - \mu (\phi_{xx} + \phi_{yy}) = 0. \quad (4)$$

We can now rewrite equation (4) in moving grids and detail the derivation. Let the moving grids be denoted by  $(\xi, \eta)$  at time  $t$ . There exists a transformation relating  $(\xi, \eta)$  and the fixed coordinates  $(x, y)$  in a one-to-one mapping as follows:

$$x = x(\xi, \eta, t), \quad (5)$$

$$y = y(\xi, \eta, t). \quad (6)$$

The material derivative of  $\phi$  is by definition expressed as

$$\begin{aligned} \frac{D\phi}{Dt} &= \left. \frac{\partial\phi}{\partial t} \right|_{(\xi,\eta)} \\ &= \left. \frac{\partial\phi}{\partial t} \right|_{(x,y)} + \left. \frac{\partial\phi}{\partial x} \frac{\partial x}{\partial t} \right|_{(\xi,\eta)} + \left. \frac{\partial\phi}{\partial y} \frac{\partial y}{\partial t} \right|_{(\xi,\eta)}. \end{aligned} \quad (7)$$

Define the grid velocity vector  $\underline{v}_g = (u_g, v_g)$  as follows:

$$u_g = \left. \frac{\partial x}{\partial t} \right|_{(\xi,\eta)}, \quad (8)$$

$$v_g = \left. \frac{\partial y}{\partial t} \right|_{(\xi,\eta)}. \quad (9)$$

We can rewrite equation (7) as

$$\left. \frac{\partial\phi}{\partial t} \right|_{(x,y)} = \left. \frac{\partial\phi}{\partial t} \right|_{(\xi,\eta)} - \nabla\phi \cdot \underline{v}_g. \quad (10)$$

The above equation provides a theoretical basis for a formulation falling within the moving grid context. Substitution of equation (10) into the target equation (4) yields

$$\left. \frac{\partial\phi}{\partial t} \right|_{(\xi,\eta)} + (u - u_g) \phi_x + (v - v_g) \phi_y - \mu (\phi_{xx} + \phi_{yy}) = 0. \quad (11)$$

Having obtained the transformation relation between fixed and moving coordinates given in (10), we can transform working equations (1)-(3) in fixed grids into their moving coordinate counterparts:

$$u_x + v_y = 0 \quad (12)$$

$$u_t + (u - u_g) u_x + (v - v_g) u_y = -p_x + \mu (u_{xx} + u_{yy}), \quad (13)$$

$$v_t + (u - u_g) v_x + (v - v_g) v_y = -p_y + \mu (v_{xx} + v_{yy}). \quad (14)$$

### Finite element analysis in moving grids

The finite element method has emerged as one of the most powerful analysis tools for simulating fluid flow problems. This method has the advantage of tackling complex geometries and accurately implementing Neumann-type boundary conditions. These attributes have provided us impetus for the utilization of this method in simulating flow in the flexible vessel.

We first consider the transport equation (11) and discretize it using a semi-discretization approach. We apply the Galerkin weighted residuals finite element model to discretize spatial derivatives through introduction of test and basis finite element spaces. Following standard finite element procedures, we can derive the corresponding ordinary differential equation as follows:

$$\underline{\underline{B}} \frac{d\phi_j}{dt} \Big|_{(\xi,\eta)} + \underline{\underline{A}} \phi_j = \underline{\underline{S}}. \quad (15)$$

We can then approximate the remaining time derivative term using the forward time-stepping scheme. The resulting algebraic system reads as

$$\frac{1}{\Delta t} \underline{\underline{B}} \phi_j^{n+1} \Big|_{(\xi,\eta)} = \underline{\underline{S}} + \left( \frac{1}{\Delta t} \underline{\underline{B}} - \underline{\underline{A}} \right) \phi_j^n \Big|_{(\xi,\eta)}. \quad (16)$$

The above Galerkin formulation provides prediction accuracy which is formally second order in space and first-order accuracy in time for cases with uniform grid size. The solution to equations (12)-(14) can be obtained using the mixed formulation. An outstanding feature of this formulation is that the pressure appears only in equations (13)-(14). This complicates the calculation of field variables from the matrix equations, which contain as many zeros as does the continuity equation in the diagonal, since eigenvalues are poorly distributed under these circumstances (Gunzburger, 1989). We denote the constrained space  $\mathcal{L}_0^2(\Omega)$  for the pressure, which consists of square integrable functions having zero mean over  $\Omega$ . In the present mixed finite element formulation, we introduce the Sobolev space  $\mathcal{H}_0^1(\Omega)$  for the velocity vector. This space consists of one square integrable derivative over  $\Omega$  and vanishes on the boundary  $\Gamma$ . Given the above finite element spaces, we seek weak solutions for  $\underline{u} \in \mathcal{H}_0^1(\Omega)$  and  $p \in \mathcal{L}_0^2(\Omega)$  from the weak statement of equations (12)-(14). In this study, the test functions  $\underline{w} \in \mathcal{H}_0^1(\Omega) \times \mathcal{H}_0^1(\Omega)$  and  $q \in \mathcal{L}_0^2(\Omega)$  are used for the vector and scalar quantities, respectively. The key element in the choice of basis functions so as to avoid node-to-node pressure oscillations is accommodation of the LBB (inf-sup or div-stability) condition (Brezzi and Douglas, 1988; Babuska, 1973; Brezzi, 1974). To get rid of this pressure mode, we employ biquadratic polynomials,  $N_i$ , to approximate  $\underline{u}$  and bilinear polynomials,  $M_i$ , to approximate  $p$ . This variable setting closely resembles the staggered mesh that is used to store the pressure and velocity unknowns in the finite volume analysis of incompressible fluid flow. The resulting ordinary equation in time is, as before, discretized using the first-order time-stepping scheme.

**Verification of the finite element formulation**

As a first step towards verifying the finite element model developed on moving grids, we consider the following variable transport equation:

$$\phi_t + 2 y \phi_x + x \phi_y - y^2 (\phi_{xx} + \phi_{yy}) = f(x,y,t). \tag{17}$$

In the above equation, the source term  $f(x)$  is chosen as

$$f(x,y,t) = e^{-t} y(2 x^3 - 2 y^3 - 3 x^2 y + 4 x y^2 - 2 x^2 - 2 y^2 + 3 x y) \tag{18}$$

so that equation (17) is amenable to the analytic solution:

$$\phi(x,y,t) = e^{-t} x (x - 1) y^2. \tag{19}$$

The problem considered is schematically shown in Figure 1. The lower boundary of the physical domain, defined in  $0 \leq x \leq 1.0$ ,  $0.5 \leq y \leq 1.5$ , varies with time from flat to its configuration according to the harmonic motion. At time  $t = 0$ , the unit square is covered with uniform grids, with a resolution of  $17 \times 17$ . The grid velocity is prescribed as follows:

$$\underline{v}_g = ( u_g , v_g ) = ( 0 , \frac{\pi}{2} \sin(2 \pi \xi) \cos(\pi t) (\eta - 1) ). \tag{20}$$

Taking the time increment  $\Delta t$  as  $10^{-4}$ , we started the calculation from  $t = 0$  and terminated at  $t = 1$ . For the problem which is subject to analytic boundary

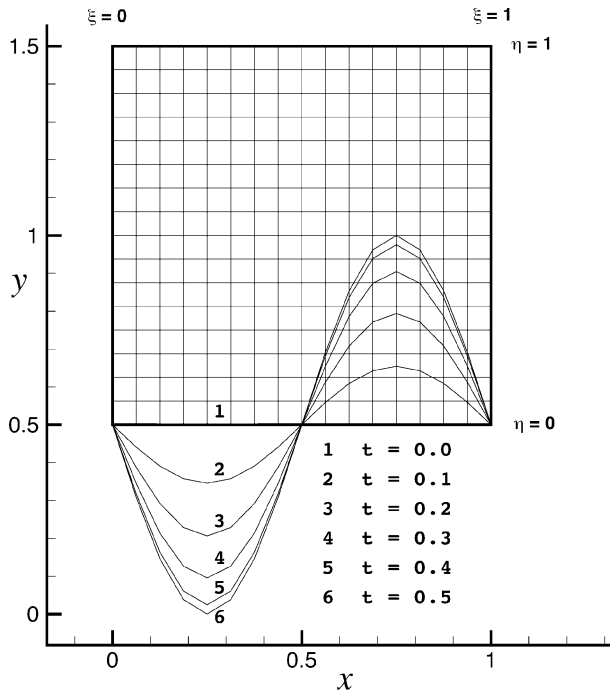


**Figure 1.**  
The schematic of the  
problem considered for  
the solution of scalar  
transport model  
equation

conditions, we measured the prediction errors in their  $L_2$ -error norms for each  $10^3$  time steps. The resulting errors are tabulated in Table I, from which it is easy to conclude that analysis conducted in moving grids has been analytically verified.

Having successfully verified the Galerkin formulation of the scalar transport equation in moving grids, we now proceed to obtain analytic verification of the Navier-Stokes code so far developed. The test problem is as follows:

$$u_x + v_y = 0 \tag{21}$$

$$u_t + u u_x + v u_y + p_x - u_{xx} - u_{yy} = f_1(x, y, t), \tag{22}$$

$$v_t + u v_x + v v_y + p_y - v_{xx} - v_{yy} = f_2(x, y, t). \tag{23}$$

The source vector  $\underline{f} = (f_1, f_2)$  for this study is chosen to be

$$f_1(x, y, t) = \frac{1}{2} e^{-2t} x (x + 1) (2x + 1) y^2 - e^{-t} (x^2 + x + 1) y, \tag{24}$$

$$f_2(x, y, t) = \frac{1}{2} e^{-2t} (2x^2 + 2x + 1) y^3 - \frac{1}{2} e^{-t} [2x(y^2 + 3) + y^2 + 2]. \tag{25}$$

Given the above source vector  $\underline{f}$ , equations (21)-(23) are amenable to the analytic solutions given below:

$$u = x (x + 1) y e^{-t}, \tag{26}$$

$$v = -\frac{1}{2} (2x + 1) y^2 e^{-t}, \tag{27}$$

$$p = x y e^{-t}. \tag{28}$$

The physical domain was initially configured as a rectangular:  $0 \leq x \leq 1.0$ ,  $0 \leq y \leq 0.5$ . To start the calculation, we uniformly discretize the domain, resulting in a grid system with a resolution of  $41 \times 21$ . This grid moved according to the grid velocity given below:

$$\underline{v}_g = ( 0, -\frac{\pi}{5} \eta \sin(2\pi\xi) \cos(\pi t) ). \tag{29}$$

Calculation started from  $t = 0$  and terminated at  $t = 1$  with a uniform time increment  $\Delta t = 10^{-2}$ . We plot prediction errors in their  $L_2$ -norm and tabulate

Time	$L_2$ norm	Time	$L_2$ norm
0.1	$1.3494526 \times 10^{-5}$	0.6	$7.0078463 \times 10^{-5}$
0.2	$2.4916741 \times 10^{-5}$	0.7	$4.7497390 \times 10^{-5}$
0.3	$4.5586862 \times 10^{-5}$	0.8	$2.2928949 \times 10^{-5}$
0.4	$6.7825187 \times 10^{-5}$	0.9	$8.9777435 \times 10^{-5}$
0.5	$7.8615689 \times 10^{-5}$	1.0	$5.1143585 \times 10^{-5}$

**Table I.**  
A summary of prediction errors for the test problem given in equations (17)-(19)

them for every ten  $\Delta t$  in Tables II and III for the pressure and velocity unknowns, respectively. To better illustrate the result, we also plot the computed and analytic pressure contours in Figure 2. As Tables II and III and Figure 2 show, it has been confirmed that the present finite element code can be applied with confidence to analysis of transient flows with a moving boundary. Given that the space conservation law plays an essential role in transient calculations with moving boundary, it is important to assure that in a cell with an area  $A$  the following property is satisfied at the discrete level:

$$\frac{d}{dt} \int_A dA - \int_S \underline{v}_g \cdot d\underline{s} = 0. \quad (30)$$

In the above,  $\underline{s}$  denotes the unit tangent along the boundary of the cell of interest and  $\underline{v}_g$  is known as the grid velocity vector.

### Computed results

Considering excellent agreement of the model predictions with all of the analytic solutions given in the previous section, the proposed method permits direct solution of the Navier-Stokes equations and can be applied with confidence to explore more complex flow phenomena. We now consider incompressible fluid flow with kinematic viscosity 0.0025 in a domain delineated by time-dependent boundaries. At  $t = 0$ , the vessel was configured to be flat. Inside the vessel, a flow was of the fully developed type with an

Time	$L_2$ norm	Time	$L_2$ norm
0.1	$0.241058 \times 10^{-3}$	0.6	$0.506236 \times 10^{-3}$
0.2	$0.342123 \times 10^{-3}$	0.7	$0.370805 \times 10^{-3}$
0.3	$0.490374 \times 10^{-3}$	0.8	$0.262840 \times 10^{-3}$
0.4	$0.595274 \times 10^{-3}$	0.9	$0.220708 \times 10^{-3}$
0.5	$0.599269 \times 10^{-3}$	1.0	$0.225021 \times 10^{-3}$

**Table II.**  
A summary of prediction errors for pressure in the numerical solution of equations (21)-(25)

Time	$L_2$ norm	Time	$L_2$ norm
<i><math>L_2</math>-error norm for u</i>			
0.1	$0.132936 \times 10^{-5}$	0.6	$0.658466 \times 10^{-6}$
0.2	$0.176829 \times 10^{-5}$	0.7	$0.490666 \times 10^{-6}$
0.3	$0.182225 \times 10^{-5}$	0.8	$0.916945 \times 10^{-6}$
0.4	$0.157429 \times 10^{-5}$	0.9	$0.139295 \times 10^{-5}$
0.5	$0.114449 \times 10^{-5}$	1.0	$0.169938 \times 10^{-5}$
<i><math>L_2</math>-error norm for v</i>			
0.1	$0.129945 \times 10^{-5}$	0.6	$0.718854 \times 10^{-6}$
0.2	$0.168458 \times 10^{-5}$	0.7	$0.324970 \times 10^{-6}$
0.3	$0.180234 \times 10^{-5}$	0.8	$0.568773 \times 10^{-6}$
0.4	$0.163438 \times 10^{-5}$	0.9	$0.892528 \times 10^{-6}$
0.5	$0.123798 \times 10^{-5}$	1.0	$0.104950 \times 10^{-5}$

**Table III.**  
A summary of prediction errors for velocities  $u$  and  $v$  for the numerical solution of equations (21)-(25)

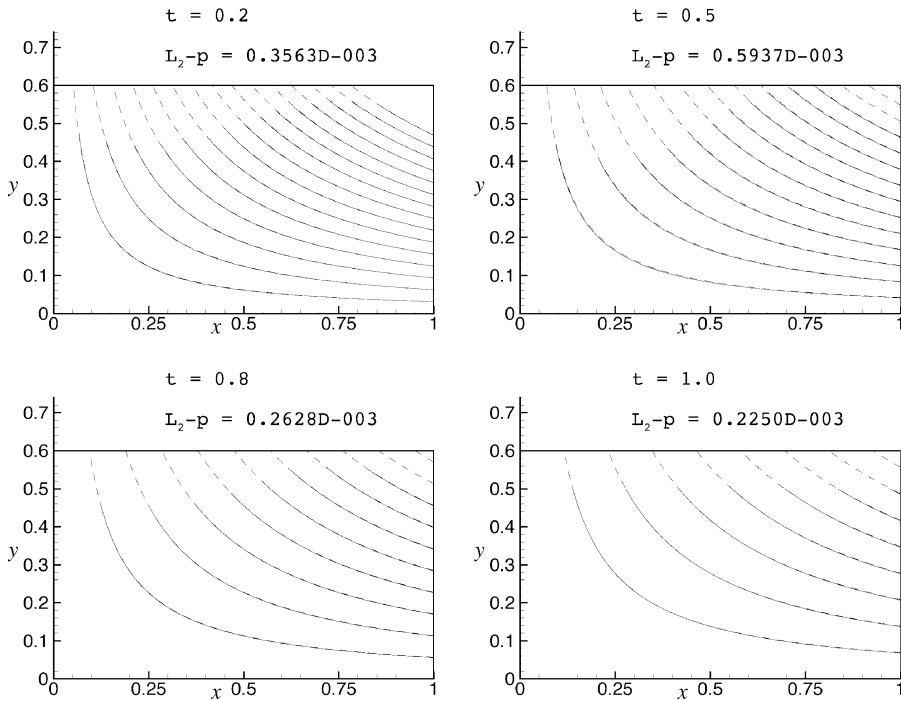


**Figure 2.**  
A comparison of  
computed (—) and  
analytic (- -) pressures  
for the solutions of  
Navier-Stokes equations

average velocity of  $u_{mean} = 2$ . This gave Reynolds number of 400. The flow under investigation falls in the laminar flow range. The test problem schematically shown in Figure 3 reveals that a part of the vessel walls was allowed to move in time. For the present study, the upper and lower collapsible vessel walls were defined a priori by the curves given below:

$$\begin{aligned}
 x &= \xi, \\
 y &= \begin{cases} \eta & ; \quad \text{else} \\ \eta - (0.2 \sin(2\pi(\xi - 1)) \sin(\omega\pi t)) & ; \quad 1 < \xi < 2 \end{cases} \quad (31)
 \end{aligned}$$

In the above,  $\omega$  denotes the frequency of the oscillating vessel wall.

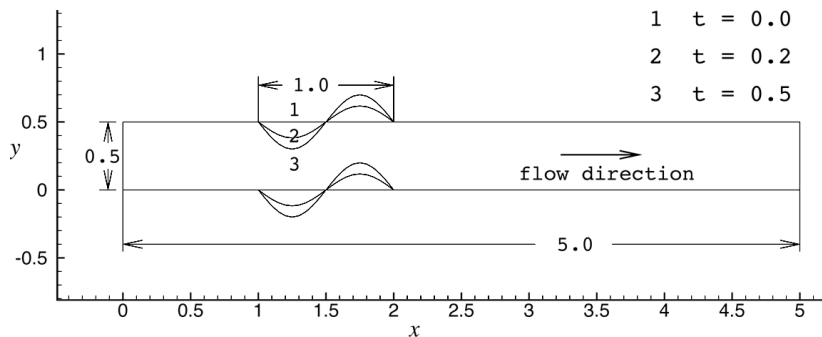


**Figure 3.**  
The schematic of the  
vessel under  
investigation

The incoming flow was fixed throughout the analysis. This is physically plausible since the inlet plane was placed sufficiently upstream of the harmonically oscillating section of the vessel. The distance downstream the perturbed vessel in which the stress-free boundary condition is applied is 5. This length was sufficiently downstream of the perturbed vessel, allowing the fluid to leave the computational domain with very little upstream influence. On physical grounds, no-slip conditions applied at the vessel wall. The grid considered here has a resolution of  $15 \times 101$  shown in Figure 4. In order for an oscillatory flow to be accurately predicted, the grid must be clustered near the vessel wall. Moreover, we demand that grids moving in time be smoothly distributed with order to avoid probable prediction deterioration due to grid distortion. Following this line, the movement of grids is prescribed according to equation (31).

As is typical with the numerical analysis of flow problems, a grid independent test is conducted to justify that the grid is properly chosen. To this end, the model was run on a domain of three grid resolutions. In this study,  $11 \times 61$ ,  $19 \times 321$ ,  $35 \times 641$  nodes are considered in the  $x$  and  $y$  direction, respectively. The results obtained for three investigated grids are plotted at the same selected sections shown in Figure 5. Observation of the presented  $u$  and  $v$  profiles in Figures 5(a) and 5(b), respectively, indicates that they follow the same trend. The difference observed at the chosen sections is negligibly small. This implies that the grid with  $15 \times 101$  nodes is sufficient to describe the flow and this grid will be used in the following discussion of results. To obtain a faithful record of the flow development, we begin our presentation of results by plotting a sequence of pressure contour plots and streamlines in Figure 6. This plot shows that the flow subject to the oscillating boundary has a rich and complex structure. Much more detailed study of results will be required before the physical phenomenon can be fully understood.

We also plot in Figure 7 the streamlines at the start of the flow development, say at  $t = 0.02$ . Clearly evident from this figure is that the streamlines intersect with the vessel wall only in the collapsible portion. The reason for this distinct flow feature is attributed to the vessel velocity whose normal component is not zero at the oscillatory vessel wall. Discussion of the results will be followed by illustration of the complex and rapidly changing features of the transient flow. As the vessel's harmonic motion commences, the external energy added to the flow causes the flow pattern to vary. Because the vessel varies harmonically in time, the flow passage becomes increasingly wavy, leading to eddy formation

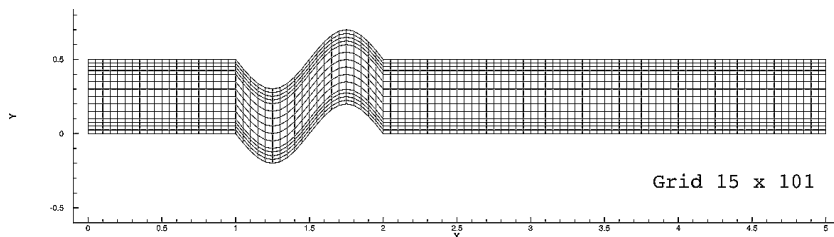


**Figure 4.**  
An illustrative example  
of the grid for the  
calculation of problem  
under investigation

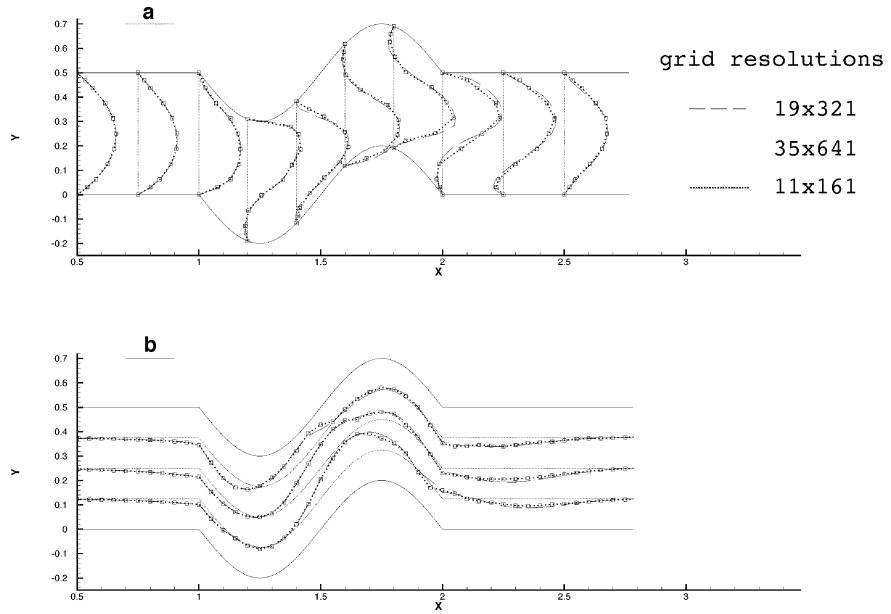


**Figure 5.** Grid independence test on three grids of different resolutions, (a)  $u$  velocity profiles; (b)  $v$  velocity profiles

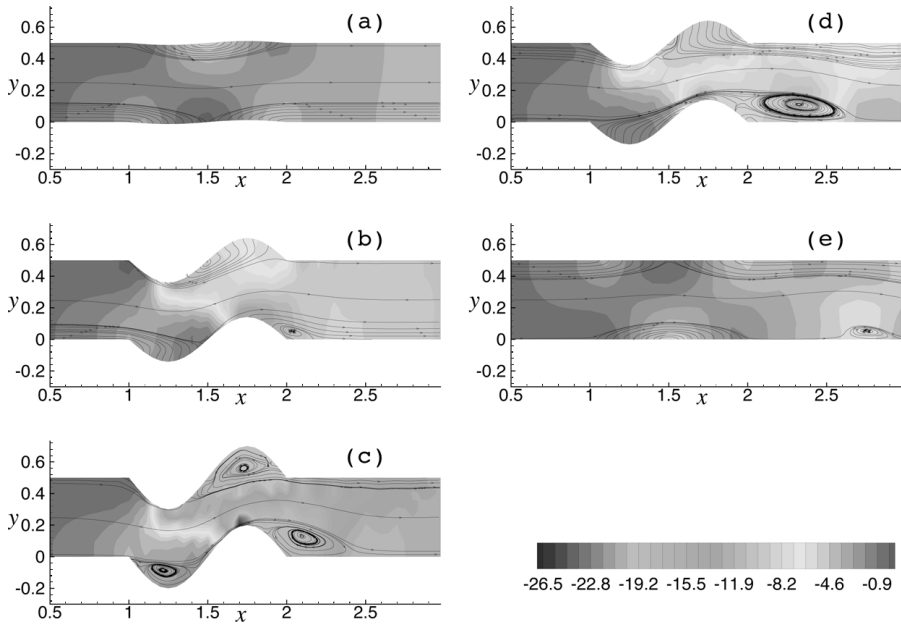


**Figure 6.** Time evolving plots of pressure contours and streamlines in the vessel at (a)  $t = 0.02$ ; (b)  $t = 0.25$ ; (c)  $t = 0.5$ ; (d)  $t = 0.75$ ; (e)  $t = 1.0$

in regions where the flow undergoes expansion. As time progresses, the accompanying centrifugal force is sustained in the wavyly configured vessel and plays an increasingly important role on the time-evolving flow structure. It is seen that “vortex A” grows in size and intensity.

As time is increased further, three vortices can be clearly seen in Figure 8 at  $t = 0.5$ . For the sake of description, we still call these vortices “vortex A”, “vortex B”, and “vortex C”. In the approach to the convexly configured cavity on the lower vessel wall, the incoming flow fills in. Fluid particles which are entrained to “vortex A” encounter a higher pressure in regions around the right end of the cavity. The direct consequence of this high pressure region is an upstream flow motion, which causes the recirculating flow to appear in “vortex A”. This eddy formation is mainly due to the concavely configured vessel. It is seen that this eddy vanishes as the vessel turns flat again in the subsequent harmonic motion. While the cavity where “vortex B” resides assumes a similar shape to that where “vortex A” is located, the formation of “vortex B” takes a different evolving route. “Vortex B” is seen to occur as a result of complex eddy formation and merging. As time evolves, a vortex of smaller size, as shown in Figure 8, is formed first. This is followed by forming a downstream primary eddy. In between the two eddies, there is a topological singular point, as is shown in Figure 9, called a saddle point. Owing to this critical point formed inside the cavity, it is easy to see why this vortex assumes a horse-shoe vortex shape. The main reason why the vortex formation is so different is attributed to the fact that the formation of “vortex B” is strongly affected by the local high pressure value found at the edge of “vortex A”. At a time subsequent to  $t = 0.5$ , “eddy b” will be entrained into its nearby vortex. The reason for this is that the local high pressure established near “vortex A” can no longer sustain the existence of “eddy b”.

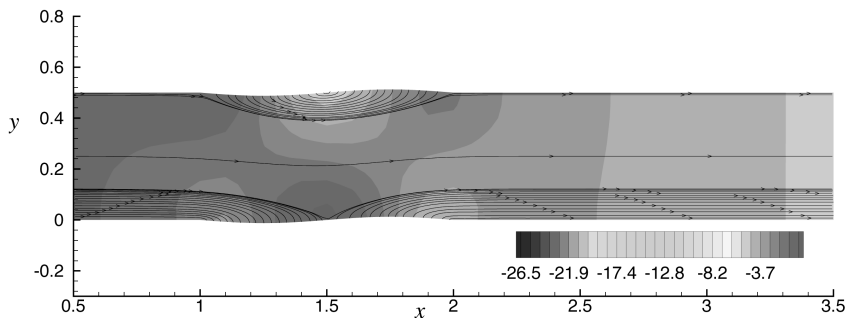


**Figure 7.**  
A plot of pressure  
contours and stream-  
lines at  $t = 0.02$

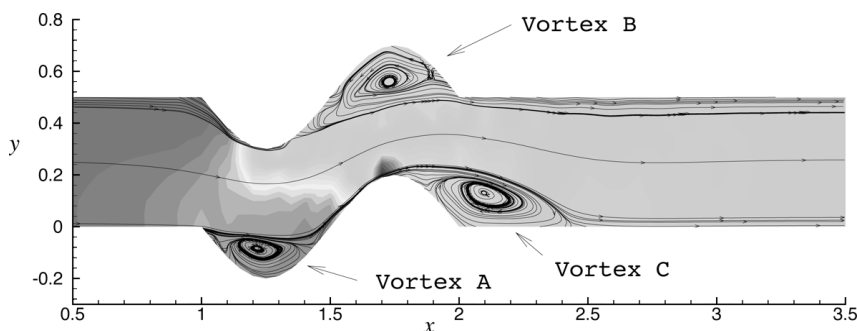
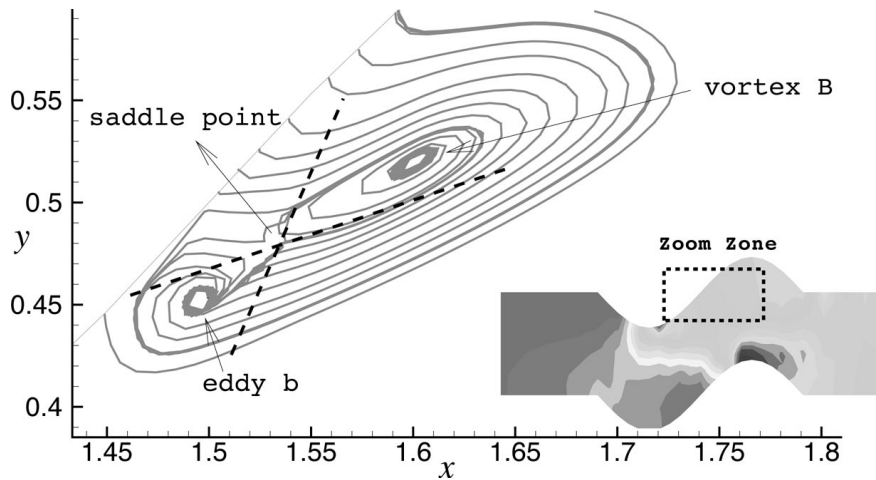


**Figure 8.**  
A plot of pressure  
contours and  
streamlines at  $t = 0.5$

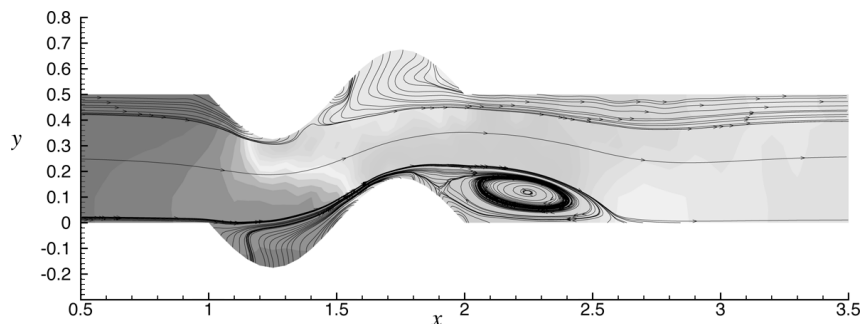
**Figure 9.**  
A clear representation of the saddle point formed in “vortex B”



The formation of “vortex C” closely resembles that of the primary vortex established behind the step in the backward-facing step problem (Armaly *et al.*, 1983). “Vortex C” occurs as a result of flow expansion. The curved incoming flow separates from the apex of the convexly configured vessel and reattaches to the flat lower vessel wall. The size and intensity of this vortex depends on the extent of deformation. It is seen that the larger the value of geometric perturbation, the larger “vortex C” becomes. This is analogous to the backward-facing step problem in that there is an increase in the reattachment length with an increase in  $h/H$ , where  $h$  and  $H$  represent the step height and the channel height, respectively. In contrast to “vortex A”, “vortex C” does not disappear immediately as the vessel wall flattens. Instead, the compressed eddy convects downstream with decreasing intensity. Eventually, the vortex motion emerging from the “vortex C” diminishes.

As Figure 6 shows, the pressure field reveals strong changes in the flow. The change is seen to maximize in the vicinity where the vessel has a larger curvature. This finding agrees with our expectation in that the pressure loss is the direct consequence of the curved flow due to the change of the vessel’s configuration. At a still later time, say at  $t = 0.66$ , the harmonically-varying

**Figure 10.**  
A plot of pressure contours and streamlines at  $t = 0.66$



vessel wall decreases in amplitude. As alluded to earlier, for fluid particles in vortices “A” and “B”, drastic changes in the flow pattern are encountered. As Figure 10 shows, streamlines intersect with the vessel walls. What is remarkable is that “vortex C” seems not to be much affected. The fluid flow which is pumped out of “vortex A” by the high pressure established on the curved lower vessel wall is not completely entrained into the main flow. Rather, this flow convects downstream and fills into “vortex C”.

### Concluding remarks

In this paper, a Galerkin finite element model has been presented for the prediction of fluid flow in a domain with moving boundaries. To facilitate the analysis, working equations have been derived in moving grids in order to adapt to the flow field. It is noteworthy that use of the geometric conservation law property is essential for analyses conducted on moving grids. In the spatial discretization, we have applied the Galerkin finite element method to obtain a second-order spatially accurate solution. The remaining ordinary differential equation, which involves time derivatives, has been discretized using the first-order accurate time-stepping method. The proposed formulation in moving grids has been analytically verified through numerical studies on scalar transport equation as well as the Navier-Stokes equations. Results have also been presented for the flow in a vessel, where a portion of the surface bounding the physical flow region moves in time. After conducting grid independent tests, the physical details obtained in this study are summarized as follows. In the flow evolution, three eddies of different characters have been found. There is an eddy which closely resembles the primary eddy behind the backward-facing step. Of the two eddies in the concavely configured cavity, one assumes a horse-shoe vortex shape. A saddle point is observed prior to the merging of two adjacent vortices of different sizes in this cavity. It is also worth noting that streamlines which are orthogonal to the moving vessel walls are observed at the beginning and at the end of the oscillatory motion.

### References

- Armaly, B.F., Durst, F., Perrira, J.C.F. and Schönary, B. (1983), “Experimental and theoretical investigation of backward-facing step flow”, *J. Fluid Mech.*, Vol. 127, pp. 473-96.
- Babuska, I. (1973), “The finite element method with Lagrangian multipliers”, *Numer. Math.*, Vol. 20, pp. 179-92.
- Brezzi, F. (1974), “On the existence, uniqueness and approximation of saddle point problem analysis from Lagrangian multipliers”, *RAIRO, Anal. Num.*, Vol. 8 No. R2, pp. 129-51.
- Brezzi, F. and Douglas, J. (1988), “Stabilized mixed methods for the Stokes problem”, *Numer. Math.*, Vol. 53, pp. 225-35.
- Demirdizic, I. and Peric, M. (1983), “Space conservation law in finite volume calculation of fluid flow”, *Int. J. Numer. Meths. in Fluids*, Vol. 8, pp. 1037-50.
- Demirdizic, I. and Peric, M. (1990), “Finite volume method for prediction of fluid flow in arbitrarily shaped domains with moving boundaries”, *Int. J. Numer. Meths. in Fluids*, Vol. 10, pp. 771-90.

- 
- Gunzburger, M.D. (1989), "Finite element methods for viscous incompressible flows", *A Guide to Theory, Practice, and Algorithms*, Academic Press, New York, NY.
- Ku, D.N., Giddens, D.P., Zarins, C.K. and Glagov, S. (1985), "Pulsatile flow and atherosclerosis in the human carotid bifurcation: positive correlation between plaque location and low and oscillatory shear stress", *Arteriosclerosis*, Vol. 5, pp. 293-302.
- Ladyzhenskaya, O. (1969), *The Mathematical Theory of Viscous Incompressible Flow*, Gordon and Breach, New York, NY.
- Satoru, O. and Tomiko, I. (1987), "A method for computing flow fields around moving bodies", *J. Comput. Phys.*, Vol. 69, pp. 49-68.
- Schouten, J.A. (1954), *An Introduction to Tensor Analysis and its Geometrical Applications*, Ricci-Calculus, Springer-Verlag, Berlin.
- Sheu, T.W.H., Tsai, S.F., Hwang, W.S. and Chang, T.M. (1999), "A finite element study of the blood flow in total cavopulmonary connection", *Computer and Fluids*, Vol. 28 No. 1, pp. 19-39.
- Taylor, C.A., Hughes, T.J.R. and Zarins, C. (1998), "Finite element modeling of blood flows in arteries", *Comput. Methods Appl. Mech. Engrg*, Vol. 158, pp. 155-96.
- Thomas, P.D. and Lombard, C.K. (1979), "Geometric conservation law and its application to flow computations on moving grids", *AIAA J*, Vol. 17 No. 10, pp. 1030-7.
- Trulio, J.G. and Trigger, K.R. (1961), *Numerical Solution of the One-dimensional Hydrodynamic Equations in an Arbitrary Time-dependent Coordinate System*, University of California Lawrence Radiation Laboratory Report UCLR-6522.